Published January 27, 2016

Original Research

Relating Quantitative Soil Structure Metrics to Saturated Hydraulic Conductivity

Dennis V. Eck, Mingming Qin, Daniel R. Hirmas,* Daniel Giménez, and Nathaniel A. Brunsell

Soil structure affects saturated hydraulic conductivity (K_s) by creating highly conductive macropores that preferentially transmit soil water. In this study, we explored the relationship between K_s and macropores in an Oxyaquic Vertic Argiudoll in northeastern Kansas. Macropores were quantified from an excavation wall using multistripe laser triangulation (MLT) scanning. Soil water contents were measured at four depths within a soil lysimeter installed within 2 m of the MLT-scanned soil profile and adjacent to an Ameriflux tower monitoring precipitation, air temperature, and solar radiation. Selected hydraulic properties of soil horizons within the lysimeter were optimized to water content data using a Markov chain Monte Carlo technique in combination with the mobile–immobile water (MIM) model in HYDRUS-1D. Estimates of K_s varied between 4198 cm d^{-1} in the A horizon and 0.6 cm d^{-1} in a 2Btss2 horizon with strongly expressed wedge structure. Approximately 87% of the variation in K_s was explained by the geometric mean of the widths of pores quantified with the MLT technique and modified by the coefficient of linear extensibility (COLE). The use of the COLE allows the widths of the macropores obtained under dry conditions to be approximated at saturation. Two models that predict K_s from either texture or water retention data resulted in K_s estimates that were similar to each other but significantly lower than K_s values predicted with MIM in horizons where structural pores dominate water flow. This technique shows a great deal of promise in better understanding and predicting the relationship of soil structure to water flow.

Core Ideas:

- Soil structure quantified in the field using a 3D laser scanning technique (MLT).
- MLT data and coefficient of linear extensibility combined into a structure metric.
- Soil water contents recorded at four depths in a field lysimeter and used in HYDRUS-1D.
- Saturated conductivity (K_s) estimated with a Markov chain Monte Carlo approach.
- New metric better correlated to K_s in horizons with strong soil structure.

Abbreviations: COLE, coefficient of linear extensibility; MIM, mobile–immobile; MLT, multistripe laser triangulation; PET, potential evapotranspiration.

Soil water flux affects many important soil and environmental processes including root water uptake, nutrient and contaminant transport, and aquifer recharge. The flux of water into and through soil can often be modeled if the hydraulic properties of the material are known. The specific hydraulic properties needed depend on the model being used to simulate water flux but most often include parameters describing the water retention curve and saturated hydraulic conductivity (K_s) (e.g., Šimůnek et al., 2013). Soil structure influences hydraulic properties near saturation because aggregation of soil particles and soil biological activity create highly conductive pores (known generically as *macropores*) that serve as preferential conduits for the transmission of soil water and have the potential to significantly alter soil hydraulic properties (Logsdon et al., 1993; Lin et al., 1999; Kutílek, 2004).

Saturated hydraulic conductivity is particularly sensitive to the abundance and size of macropores; this is demonstrated by the considerable decrease (often across several orders of magnitude) in hydraulic conductivity when macropores are excluded from measurements by the application of slightly negative potentials (Jarvis et al., 2002). Because the spatial density of macropores is relatively low, K_s should be measured in large enough soil volumes to include a representative sample of macropores to reduce variation in the measurements (Lauren et al., 1988). Consequently, quantification of soil structure and concomitant pore networks in the field could provide a means to predict "effective" K_s values

D.V. Eck, Bennett & Schulte Oil Company, Russell, KS 67665; M. Qin and D. Giménez, Dep. of Environmental Science, Rutgers Univ., New Brunswick, NJ 08901; D.R. Hirmas and N.A. Brunsell, Dep. of Geography and Atmospheric Science, Univ. of Kansas, Lawrence, KS 66045-7613. *Corresponding author (hirmas@ku.edu).

Vadose Zone J.
doi:10.2136/vzj2015.05.0083
Received 30 May 2015.
Accepted 21 Sept. 2015.

Vol. 15, Iss. 1, 2016

that are representative of a soil horizon (Rawls et al., 1993; Lilly et al., 2008). The use of subjective and/or qualitative morphological information such as in situ visual estimations of aggregate sizes, shapes, and number and/or cross-sectional area of macropores (O'Neal, 1949; McKenzie and Jacquier, 1997; Lilly et al., 2008; Schoeneberger et al., 2012) has typically led to grouping of K_s into classes (McKeague et al., 1982; Logsdon et al., 1990; McKenzie and Jacquier, 1997). By contrast, the use of objective measures of soil morphology such as macropore size measured in the field can lead to point predictions of K_s (Rawls et al., 1993). The use of objective measures of soil morphology in predictive models of K_s is more desirable, but a method to extract that information is lacking in the literature (Eck et al., 2013; Hartemink and Minasny, 2014).

Recent work, however, has shown that a novel structured-light scanning technique—known as multistripe laser triangulation (MLT)—has the ability to quantify soil structure for an entire soil profile by capturing the geometric information of interpedal pore spaces in the field (Eck et al., 2013). With MLT, a laser scanner monitors the apparent deformation of parallel vertical laser stripes as they sweep across a surface and computes distances by detecting variations in the light intensity of the projected laser stripes (Knighton et al., 2005; Platt et al., 2010). The resulting digital data are a triangulated irregular network with areas of missing data where a return was not detected by the scanner. Eck et al. (2013) termed these areas of missing data *scan surface gaps* and used them to quantitatively characterize soil structure geometries. These scan surface gaps can be interpreted as macropores. Thus, MLT scanning opens up the potential for directly examining the relationship between macropores and K_s. For instance, Eck (2014) conducted a dye study on an undisturbed core followed by splitting the sample and scanning the inside using MLT. The macropores determined using this technique visually matched the preferential flow pathways (Fig. 1).

Considering the heterogeneity of soil morphology and related hydraulic properties near saturation, it is important to have measures of uncertainty associated with any estimate of K_s and/or water retention. Inverse modeling using multiple data types has been proposed as a way to estimate hydraulic properties and their uncertainty (Mertens et al., 2005; Vrugt et al., 2009). This approach back-calculates the hydraulic properties needed to model a measured response to flow of water through soil, such as changes in soil water content, during a certain period of time (Mertens et al., 2005). The method is particularly powerful when the state variables used for inverse modeling are measured in the field. Soil water content measured in space and time is commonly used in conjunction with measurements of pressure potential (Wöhling and Vrugt, 2011) or with field or laboratory measurements of K_s and water retention (Mertens et al., 2005; Verbist et al., 2009). The advantage of using field data for inverse modeling is that estimates of the hydraulic properties investigated are more in line with the scale or domain being modeled.

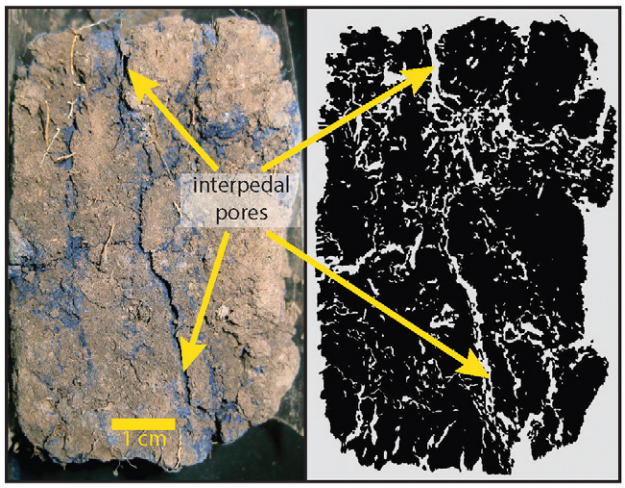

Fig. 1. Visual comparison of a dyed core section photograph (left) and multistripe laser triangulation (MLT) scan data (right) demonstrates agreement between observable conditions (dye) and captured digital data (light gray gaps). Arrows highlight several examples of interpedal pores in the core and digital data. The core sections were air dried for approximately 48 h before being split open, photographed, and scanned with an MLT scanner.

The primary objective of this work was to investigate the relationship between MLT-derived pore metrics and K_s. We derived estimates of K_s by modeling measurements of water content made in a soil lysimeter using the mobile–immobile water (MIM) model in HYDRUS-1D run with the DiffeRential Evolution Adaptive Metropolis [DREAM$_{(ZS)}$] algorithm. The DREAM$_{(ZS)}$ algorithm is a Bayesian method based on a Markov chain Monte Carlo technique that approximates the probability distribution functions of the optimized parameters from a large sample generated by interactively running a numerical model, in this case HYDRUS-1D (Vrugt et al., 2009; Wöhling and Vrugt, 2011). The resulting probability distributions provide a measure of uncertainty of the estimates. Water contents measured at several depths in the lysimeter were supplemented with water retention data at corresponding depths measured in the laboratory. This approach allowed the estimation of K_s values from each horizon present in the lysimeter together with a measure of their uncertainty. The relatively large volume of the lysimeter ensured that the estimated values were representative of the soil structure and at a similar scale to the pore metrics derived from MLT.

Materials and Methods

Study Site

This study was conducted in eastern Kansas at the site described in detail by Eck et al. (2013). Briefly, the site is located on an upland topographic position in a tallgrass prairie and oak–hickory forest ecotone (Kettle et al., 2000) that has an average annual temperature of 13.3°C and receives an average of 937 mm of annual precipitation (Brunsell et al., 2014). The soil is mapped as

a Grundy silty clay loam (a fine, smectitic, mesic, Oxyaquic Vertic Argiudoll; Soil Survey Staff, 2015) in the Nelson Environmental Study Area at the University of Kansas Field Station in Jefferson County, Kansas. This site was taken out of cultivation in the 1970s and used as a cool-season hay field until about 1987 (Foster et al., 2009; Brunsell et al., 2011). Currently, a combination of C_3 and C_4 grasses dominates the site, with a relatively minor amount of woody vegetation (Brunsell et al., 2011).

Field Lysimeter Installation and Sampling

An annular space was excavated at the site to a depth of 1 m around a column of undisturbed soil. The column was carefully hand carved to fit tightly into a 25.4-cm i.d. by 63.5-cm length stainless steel cylinder, which served as the divergence control tube for a passive capillary lysimeter (Drain Gauge G3, Decagon Devices). After reaching a depth of 75 cm, the undisturbed column was removed and a polyvinyl chloride drainage reservoir was installed beneath the original column location. The undisturbed column was repositioned on top of the drainage reservoir, with a thin layer of diatomaceous earth between the soil column and lysimeter wick to provide a good contact surface. Four soil water content and temperature sensors (5TM, Decagon Devices) were installed in the undisturbed column at depths of 5, 12, 35, and 55 cm within the lysimeter. These sensor depths corresponded to a depth within the upper horizon (5 cm), a depth at the top of the divergence control tube (12 cm), and the locations of two precut sensor slots in the divergence control tube (35 and 55 cm). Soil water content and temperature measurements were recorded on a datalogger (Em50, Decagon Devices) every 30 min using the manufacturer-recommended calibration curve. In addition, a suite of atmospheric variables, including air temperature, air pressure, solar radiation, and precipitation were also measured from an Ameriflux tower directly adjacent to the lysimeter installation (Brunsell et al., 2014). These data were used to calculate the potential evaporation (PET) from the net radiation and soil heat flux measurements using the Priestley–Taylor approach (Priestley and Taylor, 1972).

Multistripe laser triangulation data collected by Eck et al. (2013) were used for this investigation. In that study, the soil pit was extended to expose a 1-m profile and described following Schoeneberger et al. (2002). To calculate the inputs needed for modeling water flux, the root distribution was converted to an index as follows. Within each horizon, the abundance of fine and very fine roots were summed and divided by 10 to scale the final root distribution values below 1. The abundance category described in the field as "many" (i.e., $\geq$5 roots cm^{-2} on average determined from the excavation wall) was assigned a value of 5 cm^{-1}, "common" (i.e., between 1 and 5 roots cm^{-2} on average) assigned a value of 3 cm^{-1}, and "few" (i.e., <1 root cm^{-2} on average) assigned a value of 1 cm^{-1} corresponding to the lower, middle, and highest values in those categories, respectively, multiplied by the length of the assessment window (i.e., 1 cm). For example, in the 0- to 8-cm horizon, we observed many very fine and common fine roots, which were converted to a value of 0.8 cm^{-1} [i.e., (5 cm^{-1} + 3 cm^{-1})/10].

Artifacts produced during excavation of the profile were removed using a freeze method (Hirmas, 2013), and the profile was allowed to dry for 36 h to enhance the visible appearance of the soil structure (McKenzie and Jacquier, 1997; Eck et al., 2013). An MLT scanner (NextEngine Desktop 3D Scanner Model 2020i) was used to collect digital data from the profile surface as detailed by Eck et al. (2013). Triplicate bulk density samples were collected from each horizon using 3- by 5.4-cm i.d. brass rings (SoilMoisture Equipment Corp). Bulk samples and three fist-size soil clods were also collected from each horizon to analyze the particle-size distribution, organic C content, water retention, and coefficient of linear extensibility (COLE).

Laboratory Analyses

The pipette method was used to determine the particle-size distribution from the bulk samples after pretreatment to remove organic matter (Gee and Or, 2002). Bulk density was obtained from the triplicate sampled cores following Grossman and Reinsch (2002) and used to convert gravimetric water content to a volumetric basis. Other morphological and physical data from this profile (e.g., organic C content and soil structure) were obtained from Eck et al. (2013, Table 1). For each horizon, duplicate soil clods were used to measure water retention using a hanging column at −15, −30, and −60 cm. Measurement of these three points took approximately 10 d to complete. Water retention at pressure potentials lower than −60 cm were measured using bulk samples, equilibrated for 2 mo at −1000, −3000, and −10000 cm on pressure plates (four replicates) following Dane and Hopmans (2002) and using a dew-point potentiameter (WP4C, Decagon Devices) at lower pressure potentials (Leong et al., 2003; ASTM, 2003). The COLE was measured in triplicate for each horizon using the rod method following Schafer and Singer (1976). Briefly, soil samples were extruded from customized syringes as saturated pastes to form straight cylindrical rods and allowed to air dry. The COLE value was calculated as the ratio of the change in rod length between the moist and dry states to the length of the dry rod. Measured values of water content and the corresponding pressure potentials were exported to SWRC Fit (Seki, 2007) and fit with the van Genuchten (1980) water retention function:

$$S_e(h) = \frac{\theta - \theta_r}{\theta_s - \theta_r} = \left[1 + (-\alpha h)^n\right]^{-m} \quad [1]$$

where S_e is the effective saturation, θ_s and θ_r are the saturated and residual water contents, respectively, θ is the volumetric water content at equilibrium with pressure potential h, and α and n are fitting parameters. We used the common simplification that $m = 1 - 1/n$.

One-Dimensional Model of Water Flow

One-dimensional water flow through the lysimeter column was simulated with the MIM model as implemented in HYDRUS-1D (Šimůnek et al., 2013). Field-scale estimates of K_s for each soil horizon were obtained by running HYDRUS-1D with the DREAM$_{(ZS)}$ algorithm (Laloy and Vrugt, 2012; Vrugt et al., 2008, 2009). The MIM model assumes a dual-porosity system in which the soil water is partitioned between a mobile region composed of interaggregate pores (or macropores) and an immobile region where water is retained by the soil matrix and is considered stagnant (Philip, 1968; van Genuchten and Wierenga, 1976). Water retention properties for the two regions are assumed to be identical and were modeled with Eq. [1] without considering hysteresis. At any given time, the soil water content θ should fulfill the condition

$$\theta = \theta_m + \theta_{im} \quad [2]$$

where the subscripts *m* and *im* refer to the mobile and immobile regions, respectively. The water transfer rate Γ_w [T^{-1}] between the two regions is a function of the difference in effective saturation between the mobile, S_e^m, and immobile, S_e^{im}, regions:

$$\Gamma_w = \omega\left(S_e^m + S_e^{im}\right) \quad [3]$$

where ω is a first-order rate coefficient [T^{-1}].

HYDRUS-1D with the MIM model simulates water flux by numerically solving the continuity equation, which can be expressed as (Šimůnek et al., 2003)

$$\frac{\partial \theta_m}{\partial t} = \frac{\partial}{\partial z}\left[K(h_m)\frac{\partial h_m}{\partial z} - 1\right] - S(h_m) - \Gamma_w \quad [4]$$

where *t* is time, *z* is the vertical coordinate, *K* is the hydraulic conductivity, and $S(h_m)$ is a sink term assumed to be the root water uptake function. The water transfer rate can be expressed as

$$\Gamma_w = \frac{\partial \theta_{im}}{\partial t} \quad [5]$$

The hydraulic conductivity function was given by van Genuchten (1980) as

$$K\left(S_e^m\right) = K_s\left(S_e^m\right)^l \left\{1 - \left[1 - \left(S_e^m\right)^{1/(1-1/n)}\right]^{1-1/n}\right\}^2 \quad [6]$$

where *l* is a pore-connectivity parameter.

The simulation domain was the length of the lysimeter (75 cm) and contained 172 nodes with separation distances increasing linearly from approximately 0.1 cm at the surface to approximately 0.8 cm at the lower boundary. Roots were input using a relative scale by considering the abundance of fine and very fine roots as described above. The leaf area index (LAI) was obtained from MODIS satellite data at a 1-km resolution and processed to obtain the value for the pixel containing the study site (Knyazikhin et al., 1998, 1999). The satellite-derived values for LAI were 0.49 and 0.80, respectively, for the two calibration periods described below. Observation nodes were set at depths corresponding to the locations of the water content sensors (5, 12, 35, and 55 cm). The upper boundary condition was set to time-variable atmosphere conditions with runoff. Precipitation and PET data were obtained from Ameriflux tower measurements as explained above. The HYDRUS-1D Feddes root water uptake function, $S(h_m)$, with parameter values from the pasture database (Wesseling et al., 1991), were used in this work. The lower boundary condition represented the interface between the soil and a thin layer of diatomaceous earth used to increase contact with the lysimeter wick and was modeled as a seepage face in HYDRUS-1D. Initial conditions were set as pressure potentials calculated from measured water retention curves and water content data at the start of the two calibration periods used. This was done to avoid discontinuities in water content at interfaces between layers.

To reduce problems associated with non-uniqueness in the solution, we minimized the number of parameters to be optimized in HYDRUS-1D by fixing the values of five parameters: $\theta_{r,m}$, *n*, *l*, $\theta_{r,im}$, and $\theta_{s,im}$. The parameters $\theta_{r,m}$ and *l* were set at 0 (Šimůnek et al., 2001) and −1 (Schaap and Leij, 2000), respectively, across all horizons. For each horizon, values for *n* and θ_r were obtained directly from the fits of the corresponding water retention curves with Eq. [1]. Furthermore, we assumed that θ_r was equal to the residual water content of the immobile fraction, $\theta_{r,im}$, and we defined the saturated water content of that fraction, $\theta_{s,im}$, as the water content at the inflection point of the water retention curve: $\theta_{s,im} = \theta_{inf}$. Using Eq. [1] as the water retention model, θ_{inf} is calculated as (Han et al., 2008)

$$\theta_{inf} = (\theta_s - \theta_r)\left[1 + \frac{n}{n-1}\right]^{(1/n)-1} + \theta_r \quad [7]$$

The choice of defining $\theta_{s,im} = \theta_{inf}$ is based on the observation that θ_{inf} separates micro- and macroporosity (Baver, 1939; Dexter, 2004), which implies that it constitutes the upper bound of water content for the immobile region. According to this definition, porosity greater than θ_{inf} belongs to the mobile region and may not be fully captured by measurements of water retention done in clods. Consequently, we optimized $\theta_{s,m}$ (Eq.[2]) along with α (Eq. [1]), K_s (Eq. [5] and [6]), and ω (Eq. [3]).

Three Markov chains were used to run HYDRUS-1D with DREAM$_{(ZS)}$, and their convergence was determined using a scale reduction parameter, $\hat{R}$, of <1.2 for each of the optimized parameters (Wöhling and Vrugt, 2011). The DREAM$_{(ZS)}$ algorithm requires that distributions of possible values be defined a priori for each of the optimized parameters (*prior distributions*; Scharnagl

et al., 2011). Although a prior distribution can speed up the convergence of the Markov chains, our experience with preliminary runs and information by Vrugt et al. (2008) indicate that the DREAM$_{(ZS)}$ algorithm is robust even with biased prior distributions. Averages and standard deviations for α and K_s were selected from Schaap and Leij (1998, Table 4) based on the textural classes of each horizon and used to define the corresponding prior distributions, whereas mean values for $\theta_{s,m}$ were derived from the difference of measured θ_s and calculated $\theta_{s,im}$ with standard deviations of 0.1. For all horizons, values of ω were assigned a mean value of 0 and standard deviations of 0.5. Wide ranges were originally assigned to each of the parameters to ensure inclusion of the entire optimized distributions. In most cases, the DREAM$_{(ZS)}$ algorithm was run until the criteria for chain convergence was met, which means that posterior distributions were consistently within their corresponding target distribution regions. In some cases, that implied modifying prior distributions, shifting the range of parameters, and rerunning the algorithm. This strategy was used to speed the chain convergence by adjusting the prior distribution of parameters close to the target distribution. For each optimized parameter, this procedure resulted in a distribution of optimized values (*posterior distribution*), which was characterized by its median value and values representing the 2.5 and 97.5 percentiles of the distribution estimated from the cumulative distribution. The standard deviation divided by the mean value of the parameter distribution was used as a measure of the coefficient of variation (CV) and expressed as a percentage. Parameter optimization was performed using soil water contents at four depths, precipitation, and PET from two calibration time periods in April 2013 that received a total amount of precipitation of 166 mm over 9 d and 132 mm over 11 d, respectively. Because PET was similar for the two periods, they are identified based on the amount of precipitation received as period P166 (i.e., a slightly wetter period: 166 mm) and P132 (i.e., a slightly drier period: 132 mm). These relatively short periods were chosen to capture most of the range in field-measured water contents—taken just before significant rainfall events and allowed to return close to initial conditions—and to minimize temperature variation during the simulation period; Gribb et al. (2009) used two similarly short periods (8 and 5 d) to successfully estimate effective hydraulic parameters by inversion. Goodness-of-fit for both calibration runs were determined using r^2 and the root mean squared error (RMSE) estimated according to Šimůnek and Hopmans (2002):

$$r^2 = \frac{\left\{\sum w_i Y_i^{obs} Y_i^{sim} - \left[\left(\sum w_i Y_i^{obs} \sum w_i Y_i^{sim}\right)/\sum w_i\right]\right\}^2}{\left\{\sum w_i \left(Y_i^{obs}\right)^2 - \left[\left(\sum w_i Y_i^{obs}\right)^2/\sum w_i\right]\right\}} \times \frac{1}{\left\{\sum w_i \left(Y_i^{sim}\right)^2 - \left[\left(\sum w_i Y_i^{sim}\right)^2/\sum w_i\right]\right\}} \quad [8]$$

where Y_i^{obs} is the ith observation of soil water content, Y_i^{sim} is the ith simulated soil water content, w_i is the weight of the ith observations, which for this study was always equal to unity, and

$$RMSE = \sqrt{\frac{\sum_{i=1}^{n} w_i \left(Y_i^{obs} - Y_i^{sim}\right)^2}{N - M}} \quad [9]$$

where N is the number of observations and M is the number of fitted parameters.

Multistripe-Laser Triangulation and Image Analyses

As detailed by Eck et al. (2013), data collected from the MLT scans of the soil profile were processed and separated by horizon in ScanStudio HD (NextEngine Inc.) and analyzed in ImageJ (Research Services Branch, National Institute of Health). Scan data were binarized in ImageJ to exclude the solids, leaving only gaps in the digital data (referred to as pores) for analysis. Results of the image analyses were imported into R 3.0.2 (R Development Core Team) for statistical analysis, where composite metrics were calculated for each horizon following Eck et al. (2013). We excluded pores with areas <3.142 mm^2 (corresponding to the projected area of an individual coarse sand grain with a radius of 1 mm) from the analyses to separate noise from actual pores. Image metrics from each horizon were correlated with the DREAM$_{(ZS)}$-optimized K_s.

Results and Discussion

Soil Water Retention

Water retention data from each of the three methods used in this study (hanging column, pressure plate extractor, and dew-point potentiameter) followed a monotonically decreasing trend in water content with decreasing pressure potential, indicating that the measurements consistently characterized the water retention curve for each horizon (Fig. 2). The agreement between methods suggests that samples measured with the hanging column and pressure plate extractor technique reached equilibrium. The slight deviation from the monotonically decreasing trend in the 8- to 22-cm depth at approximately −23,000-cm pressure potential may be due to the higher imprecision from the dew-point potentiameter arising from increasing sensitivity to temperature at the wet end of its measurement range (Gubiani et al., 2013).

The shapes of the water retention curves (Fig. 2) reflect the increase in clay content with depth in this soil, which increases monotonically from 22% in the surface horizon to 54% in the lowest horizon (Eck et al., 2013). Water retention data plotted on a semi-logarithmic scale tended to fall on a straight line, particularly for horizons deeper than 39 cm. Also, water contents measured by the pressure plate extractor and the dew-point potentiameter techniques tended to be greater in deeper horizons, which is also a consequence of the increase in clay content with depth. Water contents measured with the dew-point potentiameter in particular are likely not to participate in the flow process.

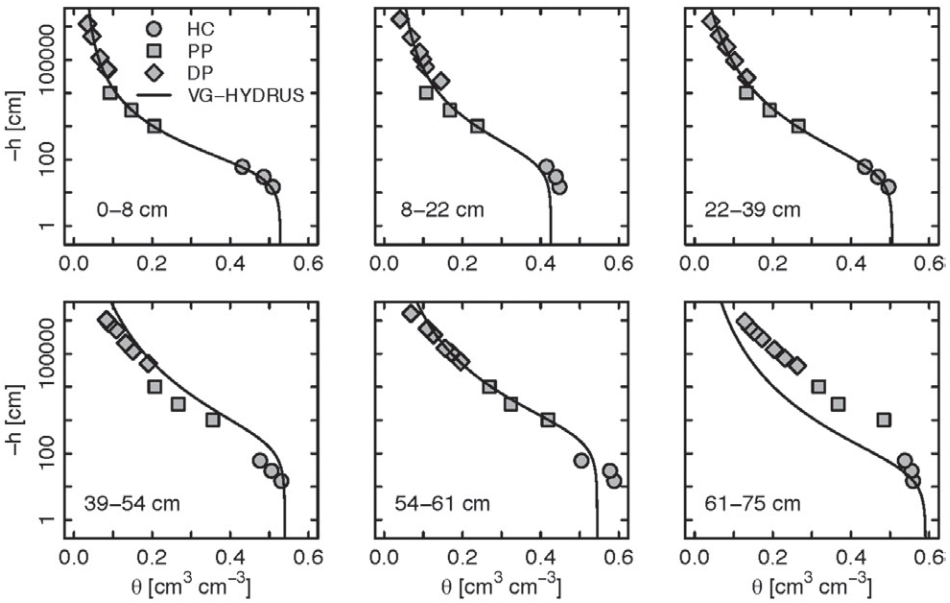

Fig. 2. Water retention curves for all horizons. Measurements were obtained using hanging column (HC), pressure plate (PP), and dewpoint potentiameter (DP) methods. Solid lines represent van Genuchten (1980) functions with the α parameter and saturated mobile water content, $\theta_{s,m}$, (i.e., $\theta_s = \theta_{s,m} + \theta_{s,im}$) optimized using the mobile–immobile water model (MIM) in HYDRUS-1D run by the DREAM$_{(ZS)}$ algorithm (VG-HYDRUS). All other water retention parameters were obtained by fitting the van Genuchten function to the measurement data using SWRC Fit (Seki, 2007).

On the other hand, water contents in the range measured by the hanging column method are influenced by a combination of soil texture and soil structure.

Modeling of Water Flow

Results of the DREAM$_{(ZS)}$-optimized HYDRUS-1D model runs for the two calibration periods showed very close agreement with measured values (Fig. 3). The r^2 values for periods P166 and P132 were 0.990 and 0.995, and the RMSE values were 0.00017 and 0.00011, respectively, indicating that water flow in both time periods was predicted reasonably well with the selected and optimized parameter values (Table 1). The CV for almost all optimized values of $\theta_{s,m}$, α, and K_s were <10%, except for K_s values from the Ap, Bt1, and Bt2 horizons during period P166, and the $\theta_{s,m}$ values from the Bt2 and 2Btss2 horizons during period P132 (Table 1). The parameter ω exhibited the largest variations, with CV values in period P132 ranging between 6.2 and 104.4%. The average difference in the values of the optimized $\theta_{s,m}$, α, and K_s between the two periods used in this study was 27%, except for values from the Bt2 and 2Btss2 horizons that had an average difference of 67.8% (Table 1). The difference between ω values of the two periods was >90% for all horizons

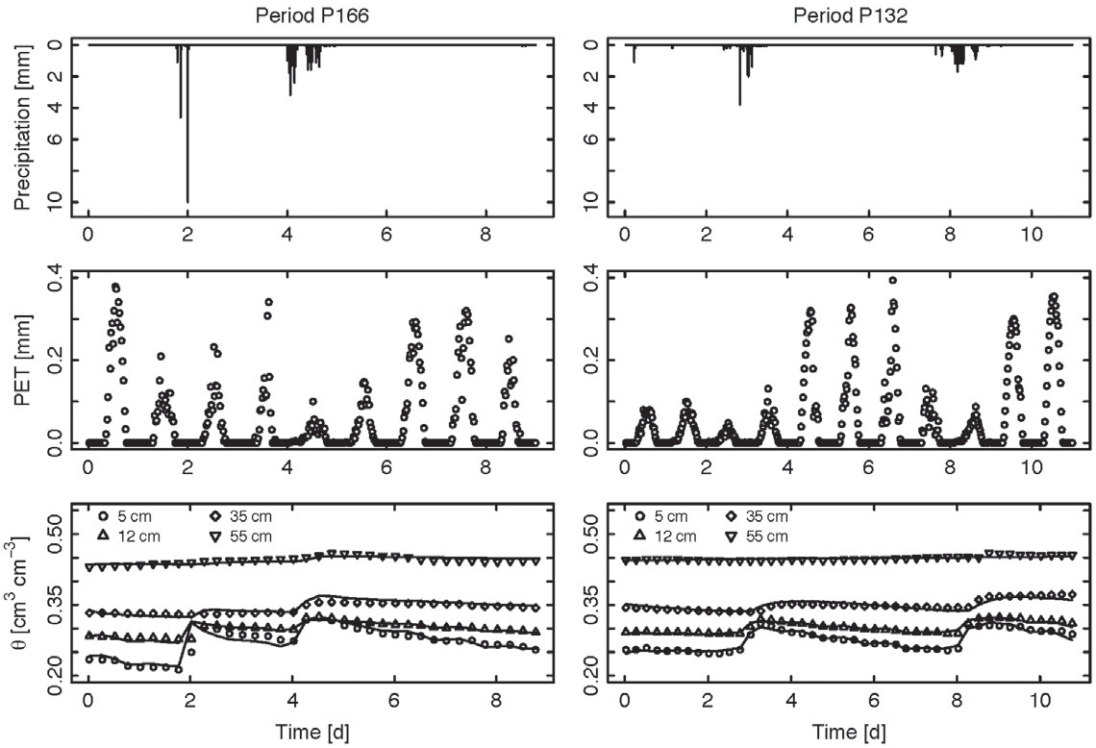

Fig. 3. Precipitation (top), potential evapotranspiration (PET, middle), and measured soil water content (θ, bottom) at four depths in the lysimeter for the two calibration periods used in this study. Solid lines in the bottom panel represent mobile–immobile water model (MIM)-optimized soil water content results from the HYDRUS-1D calibration using the DREAM$_{(ZS)}$ algorithm.

Table 1. Residual (θ_r), saturated (θ_s), saturated immobile ($\theta_{s,im}$), and saturated mobile ($\theta_{s,m}$) water contents, van Genuchten (1980) parameters α and n, transfer rate coefficient for the mobile–immobile water (MIM) model (ω), saturated hydraulic conductivity (K_s), coefficient of linear extensibility (COLE), and minimum Feret diameter (d_{Fmin}) for each horizon. Values following a ± symbol represent 1 standard deviation. The hydraulic parameters $\theta_{s,m}$, α, ω, and K_s were optimized with the HYDRUS-1D model using the DREAM$_{(ZS)}$ algorithm in the two calibration windows used in this study (periods P166 and P132). Other water retention parameters were obtained by fitting the van Genuchten function to measured data using the software SWRC Fit (Seki, 2007). Also shown are the values representing the 2.5 and 97.5 percentiles, median, and coefficient of variation (CV) of each distribution of the DREAM$_{(ZS)}$ optimized parameters (OPs).

						$\theta_{s,m}$		log(α)			log(ω)		log(K_s)			
Horizon	Depth	Statistic	θ_r	θ_s	$\theta_{s,im}$	P166	P132	P166	P132	n	P166	P132	P166	P132	COLE	d_{Fmin}
	cm							— log(cm^{-1}) —					– log(cm d^{-1}) –			mm
Ap	0–8	OP	2.8×10^{-2}	0.528	0.368	0.167	0.154	−1.717	−1.620	1.340	−2.206	−0.849	3.107	3.210	0.054 ± 0.008	2.952 ± 1.541
		2.5 percentile				0.161	0.157	−1.735	−1.588		−2.233	−0.908	3.055	3.173		
		Median				0.167	0.171	−1.719	−1.577		−1.992	−0.877	3.155	3.195		
		97.5 percentile				0.173	0.182	−1.703	−1.542		−1.833	−0.816	3.251	3.226		
		CV				1.79	3.83	1.85	4.07		22.29	6.64	11.60	3.37		
A	8–22	OP	3.7×10^{-2}	0.426	0.328	0.094	0.102	−2.068	−1.971	1.290	−2.384	−1.154	3.517	3.729	0.040 ± 0.001	2.628 ± 1.490
		2.5 percentile				0.093	0.104	−2.073	−1.950		−2.491	−1.326	3.517	3.713		
		Median				0.097	0.110	−2.053	−1.939		−2.183	−1.256	3.543	3.732		
		97.5 percentile				0.101	0.116	−2.032	−1.913		−1.991	−1.172	3.571	3.746		
		CV				2.08	2.78	2.42	3.36		27.45	10.08	3.28	2.16		
Bt1	22–39	OP	4.1×10^{-8}	0.505	0.368	0.114	0.162	−1.802	−1.634	1.222	−1.947	−0.414	0.825	1.247	0.064 ± 0.004	2.531 ± 1.594
		2.5 percentile				0.115	0.161	−1.806	−1.635		−1.954	−0.424	0.836	1.230		
		Median				0.121	0.164	−1.782	−1.630		−1.639	−0.376	0.904	1.255		
		97.5 percentile				0.127	0.167	−1.761	−1.616		−1.465	−0.322	0.997	1.275		
		CV				2.54	1.04	2.68	1.79		26.25	6.17	10.41	2.81		
Bt2	39–54	OP	4.2×10^{-6}	0.539	0.386	0.187	0.120	−2.475	−2.200	1.178	−2.375	−3.715	1.551	−0.563	0.099 ± 0.017	2.594 ± 1.474
		2.5 percentile				0.172	0.080	−2.485	−2.216		−5.233	−4.256	1.310	−0.603		
		Median				0.209	0.102	−2.452	−2.210		−2.377	−3.491	1.400	−0.574		
		97.5 percentile				0.243	0.120	−2.415	−2.193		−1.799	−3.302	1.509	−0.538		
		CV				8.78	10.66	4.16	2.20		89.46	42.09	12.54	4.18		
Btss1	54–61	OP	5.4×10^{-7}	0.545	0.405	0.118	0.160	−2.661	−2.410	1.203	−5.851	−0.993	1.436	1.505	0.121 ± 0.018	3.079 ± 1.762
		2.5 percentile				0.117	0.155	−2.669	−2.424		−6.359	−1.184	1.397	1.412		
		Median				0.121	0.159	−2.643	−2.416		−3.733	−0.968	1.433	1.476		
		97.5 percentile				0.126	0.163	−2.613	−2.398		−3.111	−0.824	1.474	1.545		
		CV				1.84	1.53	3.40	2.48		97.64	20.82	4.58	8.83		
2Btss2	61–75	OP	1.6×10^{-7}	0.591	0.404	0.257	0.116	−1.836	−1.148	1.186	−1.295	−1.459	0.837	−1.217	0.116 ± 0.015	3.008 ± 1.688
		2.5 percentile				0.212	0.080	−1.852	−1.143		−1.452	−3.910	0.793	−1.217		
		Median				0.244	0.130	−1.819	−1.137		−0.870	−1.509	0.860	−1.175		
		97.5 percentile				0.280	0.173	−1.783	−1.119		−0.636	−0.803	0.936	−1.136		
		CV				7.16	19.13	4.12	2.17		37.90	104.37	8.77	5.04		

except the 2Btss2 horizon, which was 32%. Large variations in ω were also reported by Šimůnek et al. (2001) in upward infiltration measurements that were repeated under different lower boundary pressure potentials on the same sample and by Köhne et al. (2004) in tracer displacement experiments done on two replicated columns. For horizons Bt1 and Btss1, values of $\theta_{s,m}$ were larger for period P132, which received less precipitation with similar PET values. Small differences were observed between the $\theta_{s,m}$ values of the two periods for either the Ap or A horizon, which were characterized by low COLE values (Table 1). This suggests that under relatively dry conditions, the porosity and K_s of the mobile region increased, possibly because of soil shrinkage. The exceptions of horizons Bt2 and 2Btss2 may have been caused by the lack of observations at these two horizons and, in the case of the 2Btss2 horizon, by the uncertainty of the lower boundary condition. Most optimized parameters showed consistency between the two calibration periods despite difficulties in reaching convergence (Table 1), particularly for P132, where 2 out of 24 parameters had $\hat{R}$ values >1.20 ($\hat{R}$ = 1.25 for K_s of the A horizon and $\hat{R}$ = 1.22 for ω of the 2Btss2 horizon). The variability of these distributions and the difference in values obtained in the two periods can be considered small and provide confidence in the accuracy of the optimized values from the Markov chain Monte Carlo approach used in this study.

Saturated Hydraulic Conductivity and Multistripe Laser Triangulation Derived Parameters

The K_s values optimized from the two calibration runs shown in Fig. 3 are presented in Table 1. The high conductivities of the upper three horizons are reflected in the rapid rise in water content at the 5-, 12-, and 35-cm measurement depths in response to the two rainfall events occurring at approximately Days 2 and 4 in the calibration period P166 and Days 3 and 8 in P132. Water reached the 55-cm depth very slowly in both periods compared with the upper three measurement depths owing to the small K_s of the Bt2 horizon directly above the sensor (Table 1). The Bt2 horizon, which showed the second lowest K_s among the horizons studied (Table 1), contained weakly expressed prismatic structures, which were detected as relatively thin vertical pores in the analyzed image (Eck et al., 2013).

Initial exploration of the image metrics revealed strong correlations between K_s, pore width variables, and COLE (Table 1). We used the geometric mean of the minimum Feret diameter, d_{Fmin}, measured on each pore as the metric describing pore width. The minimum Feret diameter is defined as the smallest distance between parallel lines around an object in two-dimensional space (Ferreira and Rasband, 2012; Fig. 4a). The COLE describes the potential for soil swelling by relating the change in lengths between dry and moist states to the dry soil length (Grossman and Reinsch, 2002; Soil Survey Laboratory Staff, 2004). These

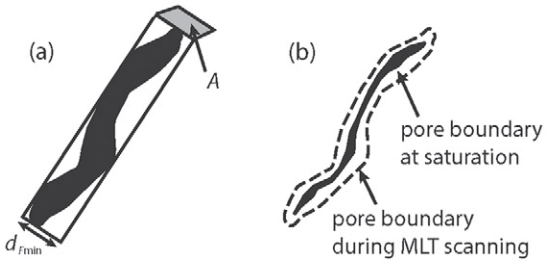

Fig. 4. Hypothetical scanned pore illustrating (a) the minimum Feret diameter measurement, d_{Fmin}, and (b) how the pore boundary would change for high shrink–swell soil materials (i.e., high coefficient of linear extensibility values) under saturated conditions compared with the relatively dry state of an excavation wall during multistripe laser triangulation (MLT) scanning. The light gray box drawn in perspective represents the area, A, generated by squaring $d_{F\,min}$.

values increased with depth from 0.05 in the surface horizon to 0.12 in the lowest two horizons corresponding to the visible presence of slickensides in those horizons (Table 1). By contrast, d_{Fmin} decreased from a surface value of 3.0 mm to <2.6 mm in the Bt1 and Bt2 horizons before increasing to 3.1 mm in the Btss1 horizon (Table 1). The COLE values for the uppermost and two lowest horizons correspond to the presence of moderately expressed granular and moderately to strongly expressed wedge structures, respectively, with clear and distinct pores in the MLT-derived images (Eck et al., 2013).

McKenzie and Jacquier (1997) argued that because morphological descriptions are conducted under relatively dry soil conditions, the metrics of visible soil pores are not representative of those pores under saturated conditions for soils with moderate or large potential for swelling. Because MLT scanning was conducted on the dry excavation wall, we normalized d^2_{Fmin} by COLE to correct for the effect of soil swelling on pore area, as illustrated in Fig. 4b. Thus, the effective pore area index, A_{eff}, corresponds to a COLE-adjusted flow cross-sectional area of the pore (Fig. 5):

$$A_{eff} = \frac{d^2_{Fmin}}{COLE} \quad [10]$$

The effect of dividing the d^2_{Fmin} value by COLE is to reduce the effective pore area of the Bt2 horizon relative to the rest of the profile (Fig. 5). The COLE values of the lowest two horizons reduced the effective pore area despite the higher d_{Fmin} of those horizons, bringing them in line with the trend observed in Fig. 5. Thus, the normalization of d^2_{Fmin} by COLE appears to effectively adjust the flow cross-sectional area of the macropores to their areas at a saturated state.

Figure 5 presents the optimized K_s estimates (HYDRUS) from the calibration run as a function of A_{eff}. A significant ($P < 0.01$) correlation between A_{eff} and K_s can be observed, and the high coefficient of determination ($r^2 = 0.869$) suggests that d_{Fmin} from the MLT-derived image represents a useful proxy of mean

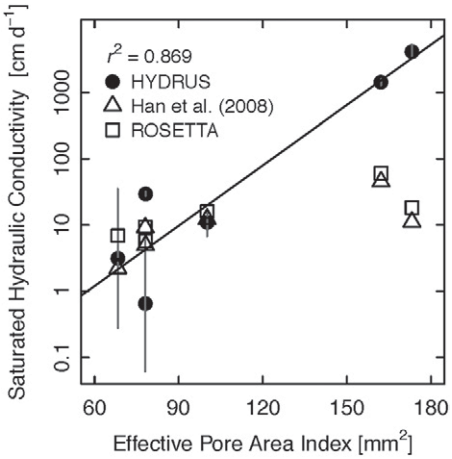

Fig. 5. Saturated hydraulic conductivity, K_s, optimized using the mobile–immobile water model (MIM) model in HYDRUS-1D as a function of effective pore area index, A_{eff}, for each soil horizon (black circles). Open triangles and squares represent K_s predictions using the Han et al. (2008) model and ROSETTA pedotransfer function, respectively. Solid gray vertical lines represent the range of K_s predictions from the two calibration periods.

macropore width. We also found a significant ($P = 0.03$) relationship between K_s and 1/COLE, with an $r^2 = 0.747$, indicating that d_{Fmin} explains approximately 12% of the variation in the K_s of the horizons used in this study. The variation explained by d_{Fmin} is considerably larger than improvements obtained by incorporating subjective measures of soil structure in the prediction of K_s (Lilly et al., 2008) or water retention at −33 and −1500 kPa (Rawls and Pachepsky, 2002).

Prediction models of K_s include pedotransfer functions based on texture (e.g., Rawls et al., 1982; Schaap et al., 2001) and models based on water retention data (e.g., Mishra and Parker, 1990; Guarracino, 2007; Han et al., 2008; Nasta et al., 2013). To assess the performance of these models with data collected in this study, we estimated K_s with the model ROSETTA (Schaap et al., 2001) based on texture and with the model proposed by Han et al. (2008) that uses water retention parameters, in this case those fitted to water retention data and optimized by DREAM$_{(ZS)}$ (Table 1). Han et al. (2008) defined macroporosity as the difference $\theta_s - \theta_{inf}$, which is equivalent to the mobile porosity defined from the water retention function in this study. Predictions with these two models provided reasonable estimates of the lowest K_s values but failed to predict the large K_s of the upper three horizons (Fig. 5), suggesting that the conductivity of these horizons is mostly driven by soil structure. These models invert the K_s of the upper two horizons largely because of clay content, whereas the A_{eff} for these horizons suggest that the A horizon should indeed have a larger K_s than the Ap horizon. Although these results do not constitute a formal comparison among different approaches to predict K_s, they highlight the value of quantifying soil morphology in enhancing understanding and prediction of hydraulic properties.

Conclusions

This study utilized a field-based quantified description of macropores obtained from MLT scanning in combination with a set of soil hydraulic properties optimized with DREAM$_{(ZS)}$ to investigate the relationship between soil structure and saturated hydraulic conductivity. We found that the geometric mean of d_{Fmin} derived from measurements made with the MLT scanning, when combined with COLE, was able to explain 87% of the variation in K_s. The use of COLE allowed the MLT-derived pore width metric (i.e., d_{Fmin}), which was obtained under relatively dry conditions from the excavation wall, to be estimated at a saturated state appropriate for K_s. The combination of COLE with d_{Fmin} allows the estimation of an effective pore area index representing a COLE-modified pore area orthogonal to the presumed direction of flow. When we compared this with two models that predict K_s from either texture or water retention data, we found that these models are able to reasonably estimate the K_s in horizons with low A_{eff} where structure has a more muted role at saturation. These models, however, significantly underpredicted K_s in horizons with lower COLE values and larger pore widths where structural pores dominate the saturation-state hydraulic character of the soil. Although future work is needed to investigate the relationship of quantified macropore metrics to K_s in a broader diversity of soil types, this technique shows a great deal of promise in better understanding and predicting the role of soil structure in soil water flow.

Acknowledgments

This research was supported in part by the University of Kansas General Research Fund, the Kollmorgen Fellowship Fund, and a grant from the CGIAR Research Program on Water, Land, and Ecosystems to Dr. Daniel Giménez. The study was conducted at and supported by the University of Kansas Field Station, a research unit of the Kansas Biological Survey and the University of Kansas. We thank Dr. Dean Kettle, Aaron Koop, and Eric Zautner for their assistance with various aspects of this project. The US-KFS Ameriflux site is sponsored by the USDOE under a subcontract from DE-AC02-05CH11231.

References

ASTM. 2003. D6836-02: Test methods for determination of the soil water characteristic curve for desorption using a hanging column, pressure extractor, chilled mirror hygrometer, and/or centrifuge. ASTM Int., West Conshohocken, PA.

Baver, L.D. 1939. Soil permeability in relation to non-capillary porosity. Soil Sci. Soc. Am. Proc. 3:52–56. doi:10.2136/sssaj1939.036159950003000C0010x

Brunsell, N.A., J.B. Nippert, and T.L. Buck. 2014. Impacts of seasonality and surface heterogeneity on water-use efficiency in mesic grasslands. Ecohydrology 7:1223–1233.

Brunsell, N.A., S.J. Schymanski, and A. Kleidon. 2011. Quantifying the thermodynamic entropy budget of the land surface: Is this useful? Earth Syst. Dyn. 2:87–103. doi:10.5194/esd-2-87-2011

Dane, J.H., and J.W. Hopmans. 2002. Pressure plate extractor. In: J.H. Dane and G.C. Topp, editors, Methods of Soil Analysis. Part 4. Physical methods. SSSA Book Ser. 5. SSSA, Madison, WI. p. 688–690. doi:10.2136/sssabookser5.4.c25

Dexter, A.R. 2004. Soil physical quality: I. Theory, effects of soil texture, density, and organic matter, and effects on root growth. Geoderma 120:201–214. doi:10.1016/j.geoderma.2003.09.004

Eck, D.V. 2014. Quantitative metrics of soil structure and relationships to hydraulic properties in a Vertic Argiudoll. M.S. thesis. Univ. of Kansas, Lawrence.

Eck, D.V., D.R. Hirmas, and D. Giménez. 2013. Quantifying soil structure from field excavation walls using multistripe laser triangulation scanning. Soil Sci. Soc. Am. J. 77:1319–1328. doi:10.2136/sssaj2012.0421

Ferreira, T., and W. Rasband. 2012. ImageJ user guide, IJ 1.46r. Natl. Inst. Health, Washington, DC. http://imagej.nih.gov/ij/docs/guide/user-guide.pdf.

Foster, B.L., K. Kindscher, G.R. Houseman, and C.A. Murphy. 2009. Effects of hay management and native species sowing on grassland community structure, biomass, and restoration. Ecol. Appl. 19:1884–1896. doi:10.1890/08-0849.1

Gee, G.W., and D. Or. 2002. Particle-size analysis. In: J.H. Dane and G.C. Topp, editors, Methods of soil analysis. Part 4. Physical methods. SSSA Book Ser. 5. SSSA, Madison, WI. p. 255–293. doi:10.2136/sssabookser5.4.c12

Gribb, M.M., I. Forkutsa, A. Hansen, D.G. Chandler, and J.P. McNamara. 2009. The effect of various soil hydraulic property estimates on soil moisture simulations. Vadose Zone J. 8:321–331. doi:10.2136/vzj2008.0088

Grossman, R.B., and T.G. Reinsch. 2002. Bulk density and linear extensibility. In: J.H. Dane and G.C. Topp, editors, Methods of soil analysis. Part 4. Physical methods. SSSA Book Ser. 5. SSSA, Madison, WI. p. 201–228. doi:10.2136/sssabookser5.4.c9

Guarracino, L. 2007. Estimation of saturated hydraulic conductivity K_S from the van Genuchten shape parameter α. Water Resour. Res. 43:W11502. doi:10.1029/2006wr005766

Gubiani, P.I., J.M. Reichert, C. Campbell, D.J. Reinert, and N.S. Gelain. 2013. Assessing errors and accuracy in dew-point potentiometer and pressure plate extractor measurements. Soil Sci. Soc. Am. J. 77:19–24. doi:10.2136/sssaj2012.0024

Han, H., D. Gimenez, and A. Lilly. 2008. Textural averages of saturated soil hydraulic conductivity predicted from water retention data. Geoderma 146:121–128. doi:10.1016/j.geoderma.2008.05.017

Hartemink, A.E., and B. Minasny. 2014. Towards digital soil morphometrics. Geoderma 230–231:305–317. doi:10.1016/j.geoderma.2014.03.008

Hirmas, D.R. 2013. A simple method for removing artifacts from moist fine textured soil faces. Soil Sci. Soc. Am. J. 77:591–593. doi:10.2136/sssaj2012.0418n

Jarvis, N.J., L. Zavattaro, K. Rajkai, W.D. Reynolds, P.A. Olsen, M. McGechan, et al. 2002. Indirect estimation of near-saturated hydraulic conductivity from readily available soil information. Geoderma 108:1–17. doi:10.1016/S0016-7061(01)00154-9

Kettle, W.D., P.M. Rich, K. Kindscher, G.L. Pittman, and P. Fu. 2000. Land use history in ecosystem restoration: A 40-year study in the prairie–forest ecotone. Restor. Ecol. 8:307–317. doi:10.1046/j.1526-100x.2000.80043.x

Knighton, M.S., D.S. Agabra, W.D. McKinley, J.Z. Zheng, D.D. Drobnis, J.D. Logan, et al. 2005. Three dimensional digitizer using multiple methods. US Patent 6980302 B2. Date issued: 27 December.

Knyazikhin, Y., J. Glassy, J.L. Privette, Y. Tian, A. Lotsch, Y. Zhang, et al. 1999. MODIS leaf area index (LAI) and fraction of photosynthetically active radiation absorbed by vegetation (FPAR) product (MOD15) algorithm. Theor. Basis Doc. NASA Goddard Space Flight Ctr., Greenbelt, MD.

Knyazikhin, Y., J.V. Martonchik, R.B. Myneni, D.J. Diner, and S.W. Running. 1998. Synergistic algorithm for estimating vegetation canopy leaf area index and fraction of absorbed photosynthetically active radiation from MODIS and MISR data. J. Geophys. Res. 103:32257–32274. doi:10.1029/98JD02462

Köhne, J.M., S. Köhne, B.P. Mohanty, and J. Šimůnek. 2004. Inverse mobile–immobile modeling of transport during transient flow. Vadose Zone J. 3:1309–1321. doi:10.2136/vzj2004.1309

Kutílek, M. 2004. Soil hydraulic properties as related to soil structure. Soil Tillage Res. 79:175–184. doi:10.1016/j.still.2004.07.006

Laloy, E., and J.A. Vrugt. 2012. High-dimensional posterior exploration of hydrologic models using multiple-try DREAM$_{(ZS)}$ and high-performance computing. Water Resour. Res. 48:W01526.

Lauren, J.G., R.J. Wagenet, J. Bouma, and J.H.M. Wosten. 1988. Variability of saturated hydraulic conductivity in a Glossaquic Hapludalf with macropores. Soil Sci. 145:20–28. doi:10.1097/00010694-198801000-00003

Leong, E.C., S. Tripathy, and H. Rahardjo. 2003. Total suction measurement of unsaturated soils with a device using the chilled-mirror dew-point technique. Geotechnique 53:173–182. doi:10.1680/geot.2003.53.2.173

Lilly, A., A. Nemes, W.J. Rawls, and Y.A. Pachepsky. 2008. Probabilistic approach to the identification of input variables to estimate hydraulic conductivity. Soil Sci. Soc. Am. J. 72:16–24. doi:10.2136/sssaj2006.0391

Lin, H.S., K.J. McInnes, L.P. Wilding, and C.T. Hallmark. 1999. Effects of soil morphology on hydraulic properties: I. Quantification of soil morphology. Soil Sci. Soc. Am. J. 63:948–954. doi:10.2136/sssaj1999.634948x

Logsdon, S., R.R. Allmaras, L. Wu, J.B. Swan, and G.W. Randall. 1990. Macroporosity and its relation to saturated hydraulic conductivity under different tillage practices. Soil Sci. Soc. Am. J. 54:1096–1101. doi:10.2136/sssaj1990.03615995005400040029x

Logsdon, S.D., E.L. McCoy, R.R. Allmaras, and D.R. Linden. 1993. Macropore characterization by indirect methods. Soil Sci. 155:316–324. doi:10.1097/00010694-199305000-00002

McKeague, J.A., C. Wang, and G.C. Topp. 1982. Estimating saturated hydraulic conductivity from soil morphology. Soil Sci. Soc. Am. J. 46:1239–1244. doi:10.2136/sssaj1982.03615995004600060024x

McKenzie, N., and D. Jacquier. 1997. Improving the field estimation of saturated hydraulic conductivity in soil survey. Aust. J. Soil Res. 35:803–825. doi:10.1071/S96093

Mertens, J., H. Madsen, M. Kristensen, D. Jacques, and J. Feyen. 2005. Sensitivity of soil parameters in unsaturated zone modelling and the relation between effective, laboratory and in situ estimates. Hydrol. Processes 19:1611–1633. doi:10.1002/hyp.5591

Mishra, S., and J.C. Parker. 1990. On the relation between saturated conductivity and capillary retention characteristics. Ground Water 28:775–777. doi:10.1111/j.1745-6584.1990.tb01991.x

Nasta, P., J.A. Vrugt, and N. Romano. 2013. Prediction of the saturated hydraulic conductivity from Brooks and Corey's water retention parameters. Water Resour. Res. 49:2918–2925. doi:10.1002/wrcr.20269

O'Neal, A.M. 1949. Soil characteristics significant in evaluating permeability. Soil Sci. 67:403–410.

Philip, J.R. 1968. The theory of absorption in aggregated media. Aust. J. Soil Res. 6:1–19. doi:10.1071/SR9680001

Platt, B.F., S.T. Hasiotis, and D.R. Hirmas. 2010. Use of low-cost multistripe laser triangulation (MLT) scanning technology for three-dimensional, quantitative paleoichnological and neoichnological studies. J. Sediment. Res. 80:590–610. doi:10.2110/jsr.2010.059

Priestley, C.H.B., and R.J. Taylor. 1972. On the assessment of surface heat flux and evaporation using large-scale parameters. Mon. Weather Rev. 100:81–92. doi:10.1175/1520-0493(1972)100<0081:OTAOSH>2.3.CO;2

Rawls, W.J., D.L. Brakensiek, and S.D. Logsdon. 1993. Predicting saturated hydraulic conductivity utilizing fractal principles. Soil Sci. Soc. Am. J. 57:1193–1197. doi:10.2136/sssaj1993.03615995005700050005x

Rawls, W.J., D.L. Brakensiek, and K.E. Saxton. 1982. Estimation of soil-water properties. Trans. ASAE 25:1316–1320. doi:10.13031/2013.33720

Rawls, W.J., and Y.A. Pachepsky. 2002. Soil consistence and structure as predictors of water retention. Soil Sci. Soc. Am. J. 66:1115–1126. doi:10.2136/sssaj2002.1115

Schaap, M.G., and F.J. Leij. 1998. Database-related accuracy and uncertainty of pedotransfer functions. Soil Sci. 163:765–779. doi:10.1097/00010694-199810000-00001

Schaap, M.G., and F.J. Leij. 2000. Improved prediction of unsaturated hydraulic conductivity with the Mualem–van Genuchten model. Soil Sci. Soc. Am. J. 64:843–851. doi:10.2136/sssaj2000.643843x

Schaap, M.G., F.J. Leij, and M.Th. van Genuchten. 2001. Rosetta: A computer program for estimating soil hydraulic parameters with hierarchical pedotransfer functions. J. Hydrol. 251:163–176. doi:10.1016/S0022-1694(01)00466-8

Schafer, W.M., and M.J. Singer. 1976. A new method of measuring shrink–swell potential using soil pastes. Soil Sci. Soc. Am. J. 40:805–806. doi:10.2136/sssaj1976.03615995004000050050x

Scharnagl, B., J.A. Vrugt, H. Vereecken, and M. Herbst. 2011. Bayesian inverse modelling of in situ soil water dynamics: Using prior information about the soil hydraulic properties. Hydrol. Earth Syst. Sci. Discuss. 8:2019–2063. doi:10.5194/hessd-8-2019-2011

Schoeneberger, P.J., D.A. Wysocki, and E.C. Benham, and Soil Survey Staff. 2012. Field book for describing and sampling soils. Version 3.0. Natl. Soil Surv. Ctr., Lincoln, NE.

Schoeneberger, P.J., D.A. Wysocki, E.C. Benham, and W.D. Broderson. 2002. Field book for describing and sampling soils. Version 2.0. Natl. Soil Surv. Ctr., Lincoln, NE.

Seki, K. 2007. SWRC fit: A nonlinear fitting program with a water retention curve for soils having unimodal and bimodal pore structure. Hydrol. Earth Syst. Sci. Discuss. 4:407–437. doi:10.5194/hessd-4-407-2007

Šimůnek, J., and J.W. Hopmans. 2002. Parameter optimization and nonlinear fitting. In: J.H. Dane and G.C. Topp, editors, Methods of soil analysis. Part 4. Physical methods. SSSA Book Ser. 5. SSSA, Madison, WI. p. 139–157. doi:10.2136/sssabookser5.4.c7

Šimůnek, J., N.J. Jarvis, M.Th. van Genuchten, and A. Gärdenäs. 2003. Review and comparison of models for describing non-equilibrium and preferential flow and transport in the vadose zone. J. Hydrol. 272:14–35. doi:10.1016/S0022-1694(02)00252-4

Šimůnek, J., M. Šejna, H. Saito, M. Sakai, and M.Th. van Genuchten. 2013. The HYDRUS-1D software package for simulating the movement of water, heat, and multiple solutes in variably saturated media. Version 4.16. HYDRUS Software Ser. 3. Dep. of Environ. Sci., Univ. of California, Riverside.

Šimůnek, J., O. Wendroth, N. Wypler, and M.Th. van Genuchten. 2001. Non-equilibrium water flow characterized by means of upward infiltration experiments. Eur. J. Soil Sci. 52:13–24. doi:10.1046/j.1365-2389.2001.00361.x

Soil Survey Laboratory Staff. 2004. Soil survey laboratory methods manual. Version 4.0. Soil Surv. Invest. Rep. 42. NRCS, Washington, DC.

Soil Survey Staff. 2015. Web soil survey. Natl. Soil Surv. Ctr., Lincoln, NE. http://websoilsurvey.nrcs.usda.gov/ (accessed 28 May 2012).

van Genuchten, M.Th. 1980. A closed-form equation for predicting the hydraulic conductivity of unsaturated soils. Soil Sci. Soc. Am. J. 44:892–898. doi:10.2136/sssaj1980.03615995004400050002x

van Genuchten, M.Th., and P.J. Wierenga. 1976. Mass transfer studies in sorbing porous media: I. Analytical solutions. Soil Sci. Soc. Am. J. 40:473–480. doi:10.2136/sssaj1976.03615995004000040011x

Verbist, K., W.M. Cornelis, D. Gabriels, K. Alaerts, and G. Soto. 2009. Using an inverse modelling approach to evaluate the water retention in a simple water harvesting technique. Hydrol. Earth Syst. Sci. 13:1979–1992. doi:10.5194/hess-13-1979-2009

Vrugt, J.A., C.J.F. ter Braak, M.P. Clark, J.M. Hyman, and B.A. Robinson. 2008. Treatment of input uncertainty in hydrologic modeling: Doing hydrology backward with Markov chain Monte Carlo simulation. Water Resour. Res. 44:W00B09. doi:10.1029/2007WR006720

Vrugt, J.A., C.J.F. ter Braak, C.G.H. Diks, B.A. Robinson, J.M. Hyman, and D. Higdon. 2009. Accelerating Markov chain Monte Carlo simulation by differential evolution with self-adaptive randomized subspace sampling. Int. J. Nonlinear Sci. Numer. Simul. 10:273–290. doi:10.1515/IJNSNS.2009.10.3.273

Wesseling, J.G., J.A. Elbers, P. Kabat, and B.J. Van den Broek. 1991. SWATRE: Instructions for input. Internal Note. Winand Staring Ctr, Wageningen, the Netherlands.

Wöhling, T., and J.A. Vrugt. 2011. Multiresponse multilayer vadose zone model calibration using Markov chain Monte Carlo simulation and field water retention data. Water Resour. Res. 47:W04510. doi:10.1029/2010wr009265